

Profile Reconstruction Utilizing Forward-Backward Time-Stepping with the Integration of Automated Edge-Preserving Regularization Technique for Object Detection Applications

Guang Yong¹, Kismet Anak Hong Ping^{1, *}, Shafrida Sahrani¹,
Mohamad Hamiruce Marhaban², Mohd Iqbal Saripan²,
Toshifumi Moriyama³, and Takashi Takenaka³

Abstract—A regularization is integrated with Forward-Backward Time-Stepping (FBTS) method which is formulated in time-domain utilizing Finite-Difference Time-Domain (FDTD) method to solve the nonlinear and ill-posed problem arisen in the microwave inverse scattering problem. FBTS method based on a Polak-Ribière-Polyak conjugate gradient method is easily trapped in the local minima. Thus, we extend our work with the integration of edge-preserving regularization technique due to its ability to smooth and preserve the edges containing important information for reconstructing the dielectric profiles of the targeted object. In this paper, we propose a deterministic relaxation with Mean Square Error algorithm known as DrMSE in FBTS and integrate it with the automated edge-preserving regularization technique. Numerical simulations are carried out and prove that the reconstructed results are more accurate by calculating the edge-preserving parameter automatically.

1. INTRODUCTION

Inverse scattering in microwave imaging has been widely studied by many researchers for last decades. Microwave imaging [1] is a very promising approach for many practical applications. It has huge potential in measuring the characteristic of the embedded objects inside a bounded space region by illuminating electromagnetic waves. Microwave imaging has the ability to retrieve information about the distribution of the dielectric properties space region, the shape and the location of the embedded object. Besides that, microwave imaging has lower cost than other well-known screening approaches, for example, positron emission tomography and computed tomography. Furthermore, microwave imaging is safer with low nonionizing radiation than X-ray mammography. Thus, it is recommended that microwave imaging is applied as a diagnostic tool for several areas which involve civil and industrial engineering [2–5], nondestructive testing and evaluation [6–10], geophysical prospecting [11] buried object detection for military [12–14] medical diagnostic for biomedical engineering [15–19], and screening tool for wood industry [20].

Solving an inverse scattering problem is a very challenging task due to nonlinearity of the scattering equations, ill-posedness of the problem and uniqueness of the solution [21]. This problem could be dealt with either in frequency-domain or time-domain. The frequency-domain based technique has successfully reconstructed satisfactory results [22, 23], but it showed some drawbacks. Firstly, the use of higher frequencies may improve the spatial resolution, but it leads to highly nonlinear formulation and more complexity when measuring the scattered field. Secondly, collected information is limited

Received 10 November 2016, Accepted 21 January 2017, Scheduled 17 February 2017

* Corresponding author: Kismet Anak Hong Ping (hpkismet@unimas.my).

¹ Applied Electromagnetic Research Group, Faculty of Engineering, Universiti Malaysia Sarawak, Kota Samarahan, Sarawak 94300, Malaysia. ² Department of Electrical and Electronic Engineering, Faculty of Engineering, Universiti Putra Malaysia, UPM Serdang, Selangor 43400, Malaysia. ³ Department of Electrical and Electronic Engineering, Faculty of Engineering, Nagasaki University 1-14 Bunkyo-machi, Nagasaki 852-8521, Japan.

when using single-frequency data. To overcome this problem, it is suggested to use time-domain based technique. Time-domain based technique has demonstrated the ability to reconstruct the distribution of dielectric properties more accurately [24–28]. Currently, time-domain based technique includes Lagrange multipliers technique by Rekanos [24], time-domain inverse scattering by Winters et al. [25] and FBTS method by Takenaka et al. [26–28].

Since the microwave imaging is a nonlinear inverse scattering problem, the adoption of regularization technique is needed to obtain a stable solution by avoiding the ill-posed nature [29, 30]. The most popular technique is using Tikhonov regularization technique to solve the ill-posed nature [31–34]. It has been applied in many different fields, and unfortunately, Tikhonov regularization strongly penalizes the discontinuities and smooths the object edges resulting blurred images. This weakness may lead to false result to the observer; for example, a doctor hardly identifies an organ or a tumor correctly due over-smoothed dielectric properties. To overcome this problem, edge-preserving regularization [26, 35] is suggested because it uses local smoothness constraints with account of intensity discontinuities.

In our previous study [36], preliminary results showed that the integration of edge-preserving regularization provided more accurate reconstructed profile. In this paper, we use bigger size and more complicated target object to prove efficiency of the Edge-preserving regularization technique. This technique is extended with automated procedures which has the ability of finding the regularization technique parameters such as weighting parameters and threshold parameters to detect the edges for each iteration. Common regularization technique parameters are exploited by numerical experiment. Based on our experiences, it is not an easy task to find those parameters for the regularization technique.

This paper is organized as follows. Section 1 introduces some challenges and problem solving of the microwave imaging approaches. Section 2 explains our proposed method, FBTS integrated with automated Edge-preserving regularization technique. Section 3 presents the numerical results and discussion. Finally, Section 4 concludes the paper.

2. METHOD

2.1. Forward-Backward Time-Stepping Method

Let us consider a region of interest (ROI) representing the 2D object embedded in a homogeneous medium. The object is assumed inhomogeneous and has different dielectric properties compared to ROI. We assume that the ROI is located in free-space medium and surrounded by 16 antennas as shown in Figure 1. Each antenna will take turn to act as a transmitter, m to transmit Gaussian pulse to ROI and the remaining antennas becoming receiver, n to receive the scattered signals until a combination of 240 transmitter/receiver data set is obtained.

The inverse scattering problem considered here is to reconstruct the dielectric profiles of the ROI

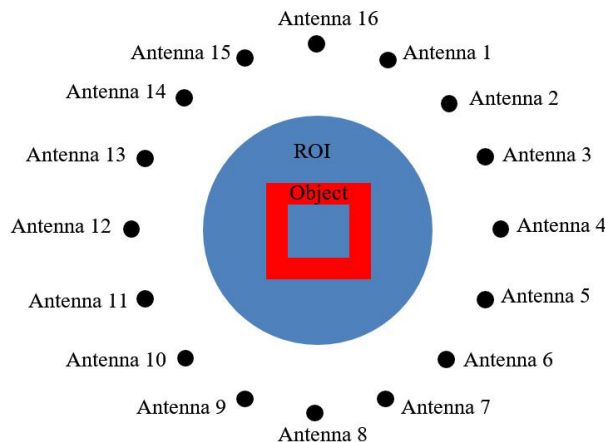


Figure 1. Configuration of the 2-D FBTS method.

by using the scattered signal collected by the receiver. In Forward-Backward Time-Stepping (FBTS) method, the collected data are formulated as an optimization problem with the form of cost functional $Q_{rec}(p)$ to be minimized as follows:

$$Q_{rec}(p) = \int_0^{cT} \sum_{m=1}^M \sum_{n=1}^N W_{mn}(t) |e_m(p; r_n, t) - \tilde{e}_m(r_n, t)|^2 d(ct) \quad (1)$$

where p is a medium parameter vector function given by

$$p = [p_1(r), p_2(r)] = [\varepsilon_r(r), \sigma(r)] \quad r = [x, y, z] \quad (2)$$

In Eq. (1), $W_{mn}(t)$ is a nonnegative weighting function which takes a value of zero at time $t = T$ (T is the time duration of the measurement), and $e_m(p; r_n, t)$ and $\tilde{e}_m(r_n, t)$ are the calculated electromagnetic fields in time domain for an estimated medium parameter vector p and the measured electromagnetic fields due to the m th source, respectively.

To find the solution of medium parameter p , a gradient-based optimization method is applied to cost functional in Eq. (1). By taking the Fréchet derivative of Eq. (1), the gradients of medium parameter vector equations are derived as

$$g_{\varepsilon_r}(r) = \int_0^{cT} \sum_{m=1}^M 2u_m(p; r, t) \frac{d}{dct} e_m(p; r, t) d(ct) \quad (3)$$

$$g_{\sigma}(r) = \int_0^{cT} \sum_{m=1}^M 2u_m(p; r, t) e_m(p; r, t) d(ct) \quad (4)$$

where $u_m(p; r, t)$ and $e_m(p; r, t)$ are the adjoint fields and electromagnetic fields calculated in the ROI, respectively. The adjoint fields, $u_m(p; r, t)$, are time reversed fields with equivalent current sources which are identical to a difference between the measured and calculated electromagnetic field data. In this paper, Polak-Ribière-Polyak conjugate gradient method is used as optimization technique to solve the inverse scattering problem.

2.2. Edge-Preserving Regularization Technique

Since the inverse scattering problem is nonlinear and ill-posed in the sense of Hadamard [37], an edge-preserving regularization technique is needed to handle this problem. Therefore, the cost functional in Eq. (1) is modified into a new total cost functional equation.

$$Q_{total}(p) = Q_{rec}(p) + Q_{edge}(p) \quad (5)$$

where the first term, $Q_{rec}(p)$, is residual term as in Eq. (1), and the second term, $Q_{edge}(p)$, is the edge-preserving regularizing term as follows:

$$Q_{edge}(p) = \lambda_{\varepsilon_r} \iint_S \varphi \left(\frac{\|\nabla p_{\varepsilon_r}\|}{\chi_{\varepsilon_r}} \right) dS + \lambda_{\sigma} \iint_S \varphi \left(\frac{\|\nabla p_{\sigma}\|}{\chi_{\sigma}} \right) dS \quad (6)$$

In this paper, Sobel operator is used to find the norm of gradient, $\|\nabla p\|$

$$\|\nabla p\| = \sqrt{p_x^2 + p_y^2} \quad (7)$$

$$p_x = \frac{1}{8} \begin{bmatrix} -1 & -2 & -1 \\ 0 & 0 & 0 \\ 1 & 2 & 1 \end{bmatrix}, \quad p_y = \frac{1}{8} \begin{bmatrix} -1 & 0 & 1 \\ -2 & 0 & 2 \\ -1 & 0 & 1 \end{bmatrix}$$

In Eq. (6), the function φ is a regularization function which has the ability for smoothing in the homogeneous areas, while edges are preserved [29, 35]. Many regularization functions have been discovered, and some well-known functions are φ_{HL} [38] and φ_{GR} [39]. In this paper, we use φ_{GM} [40] as our regularization function because it has horizontal asymptote behaviour when approaching infinity.

In dealing with the reconstruction of dielectric profile, we consider the relative permittivity ε_r and conductivity σ profile of the contrast as independent of the regularization scheme. Therefore, the edge

preserving regularization term is applied separately on the relative permittivity ε_r and conductivity σ profile. The weighting parameters λ_{ε_r} and λ_{σ} are used to balance the effect of the residual term and regularization term. The threshold parameters χ_{ε_r} and χ_{σ} are used to determine the value of the gradient norm of which discontinuity is preserved without smoothing it. Note that many researchers have used numerical observation to determine the parameters of λ and χ [26, 41].

In this work, we develop two automated procedures with a simple calculation to automatically determine the regularization technique parameters for each iteration. Firstly, the weighting parameters λ are calculated based on the gradient values of Eqs. (3) and (4), respectively. Secondly, the values of the threshold parameters χ are calculated based on half of the highest value of the norm of gradient $\|\nabla p\|$ in the ROI.

Suppose that $Q_{edge}(p)$ has a minimum in p , but to find the minimum, it is a difficult task due to nonlinearity [35]. Thus, in order to make the minimization simple, the potential function can be modified as in [42].

$$\varphi_{GM}(t) = (bt^2 + \psi(b)) \quad (8)$$

where the expression of $\psi(b)$ is $b - 2\sqrt{b} + 1$, and b is auxiliary vector also known as the discontinuity reference.

$$b_{GM} = \frac{1}{1 + (\nabla p/\chi)^2} \quad (9)$$

Then, the regularization term $Q_{edge}(p)$ can be modified into half-quadratic regularization term, $Q_{edge}(p, b)$

$$Q_{edge}(p, b) = \lambda_{\varepsilon_r} \iint_S \left[b_{\varepsilon_r} \frac{\|\nabla p_{\varepsilon_r}\|^2}{\chi_{\varepsilon_r}^2} + \psi(b_{\varepsilon_r}) \right] dS + \lambda_{\sigma} \iint_S \left[b_{\sigma} \frac{\|\nabla p_{\sigma}\|^2}{\chi_{\sigma}^2} + \psi(b_{\sigma}) \right] dS \quad (10)$$

Hence, the total cost functional will be evolved as

$$Q_{total}(p, b) = Q_{rec}(p) + Q_{edge}(p, b) \quad (11)$$

By taking the Fréchet derivative of Eq. (10), the gradients of medium parameter vector for the new edge-preserving regularization term are derived as

$$g_i(r) = -2 \frac{\lambda_i}{\chi_i^2} \nabla \cdot (b_i \nabla p_i), \quad i = \varepsilon_r, \sigma \quad (12)$$

Thus, the total gradient is obtained as

$$g_{total}(r) = g_{FBTS,i}(r) + g_{Edge,i}(r), \quad i = \varepsilon_r, \sigma \quad (13)$$

2.3. Deterministic Relaxation with Mean Square Error (DrMSE) Algorithm

In order to solve the total cost functional that expressed as in Eq. (11), we introduce alternate minimizations scheme over p and b . When the auxiliary vector b is fixed, the edge-preserving regularization term $Q_{edge}(p, b)$ is quadratic in p . Thus, the minimization of Eq. (11) can be performed by the Polak-Ribière-Polyak conjugate gradient method. When p is fixed, the values of b are analytically obtained for each point (x, y) in each profile with Eq. (9). In order to control this scheme, we propose the integration of Mean Square Error (MSE) with the deterministic relaxation processes.

$$MSE = \frac{1}{XY} \sum_{x=1}^X \sum_{y=1}^Y [p^{n+1}(x, y) - p^n(x, y)]^2 \quad (14)$$

where p^{n+1} is the current dielectric profile, p^n the previous dielectric profile, and X, Y are the point of the profile.

In this work, we are dealing with relative permittivity and conductivity profile reconstruction. Therefore, in order to reconstruct both profiles at the same time, DrMSE is introduced. To the best of our knowledge, there is no proper method to alternate this scheme reported. Most researchers have only mentioned deterministic algorithm. In the DrMSE algorithm, the MSE for each profile is calculated iteratively. When MSE for either one of the profiles is small enough, a new auxiliary vector will be estimated and applied for the minimization of Eq. (10). This procedure is repeated until the total cost functional achieves its convergence. The iterative scheme can be summarized as follows.

```

Begin, set  $n = 0$ 
Reconstruct initial profile  $p^0$ 
Reconstruct initial auxiliary vector  $b = b^0$ 
Repeat
    Reconstruct new profile  $p^{n+1}$  by minimize  $Q_{total}(p^n, b)$ 
    Compute MSE by using  $p^{n+1}$  and  $p^n$ 
    if  $MSE < 1e-6$ 
        Reconstruct new auxiliary vector  $b = b^{n+1}$ 
    Endif
Until convergence.
    
```

3. RESULTS AND DISCUSSION

In this work, we consider an object embedded in the ROI as an unknown scatterer and surrounded by 16 antennas as shown in Figure 1. In FBTS reconstruction algorithm, we use $1\text{ mm} \times 1\text{ mm}$ cell size for the FDTD lattice. The antennas will take turn to transmit sinusoidally modulated Gaussian pulse with center frequency, f_c of 2 GHz with bandwidth of 1.3 GHz. Convolutional Perfectly Matched Layer

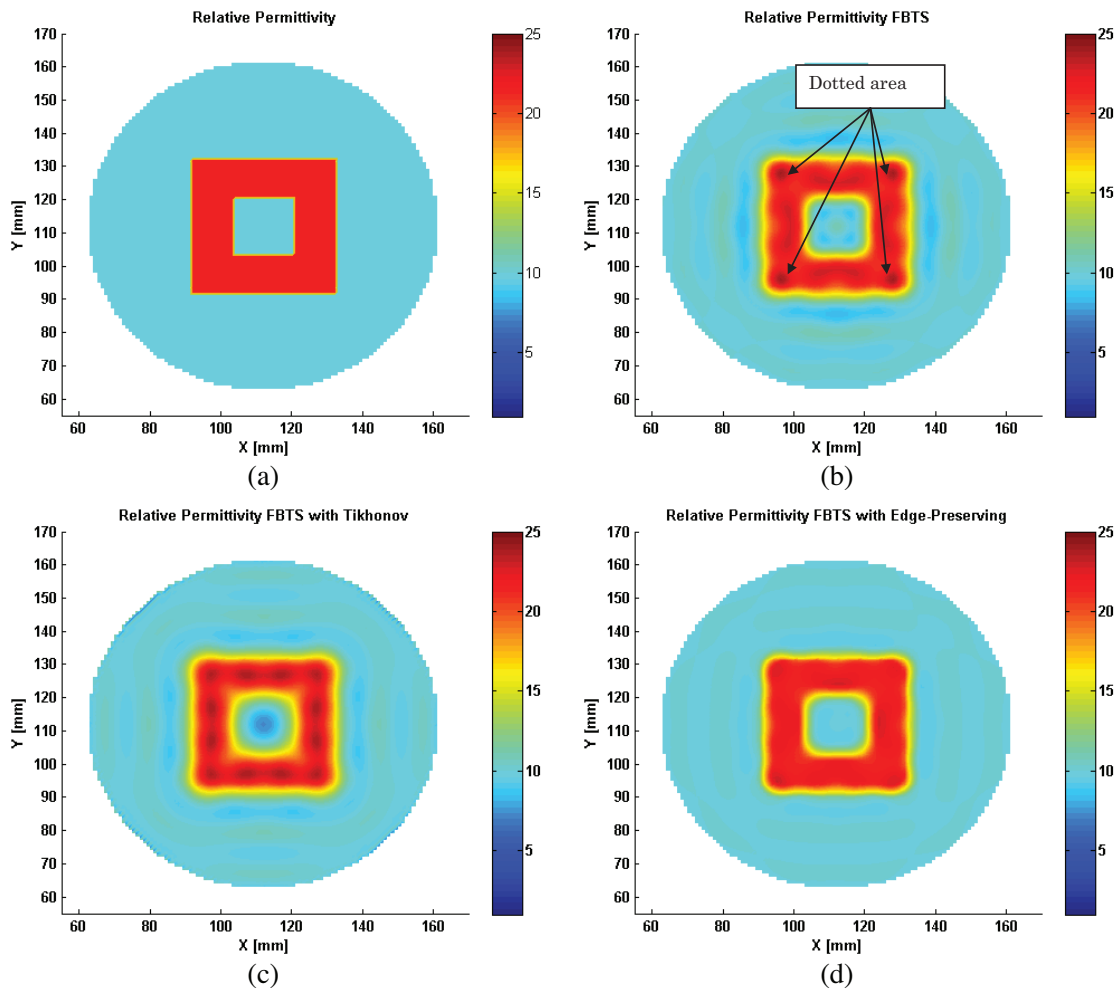


Figure 2. Relative permittivity profile: (a) Original profile. (b) Reconstructed profile by FBTS method. (c) Reconstructed profile by FBTS with Tikhonov regularization technique. (d) Reconstructed profile by FBTS with automated edge-preserving regularization technique.

(CPML) with thickness of 15 mm as an absorber is added at the borders of the FDTD lattice. This CPML has the ability to prevent the reflections of the signal at the boundary of the FDTD lattice and helps to save computation time during numerical simulation work.

In the setup, a 50 mm radius circular shape ROI with the relative permittivity $\varepsilon_r = 9.98$ and conductivity $\sigma_r = 0.18$ S/m is immersed in a free-space medium. A 20 mm \times 20 mm rectangular shape with a 8 mm \times 8 mm void rectangular shape of object is embedded at the center of ROI. This object has the relative permittivity of 21.45 and conductivity of 0.45 S/m. Assume that a *priori* known profile with the relative permittivity of 13.7 and the conductivity of 0.18 S/m which is slightly near the original profile of ROI as initial guess p^0 .

In this work, all numerical simulations are carried out up to 200 iterations. The original profile, FBTS reconstructed profile, FBTS with Tikhonov regularization technique reconstructed profile and FBTS with automated Edge-preserving regularization technique reconstructed profile images for the object relative permittivity spatial distribution are illustrated in Figure 2. Figure 3 shows the corresponding conductivity spatial distribution. As shown in Figure 2 and Figure 3, all these techniques have successfully reconstructed the location and shape of the embedded object in ROI. However, there are enormous different reconstructed profile images for these three techniques.

In FBTS method, the reconstructed profile successfully points out the location and shape of the embedded object. However, for the reconstructed relative permittivity profile, some dotted areas at

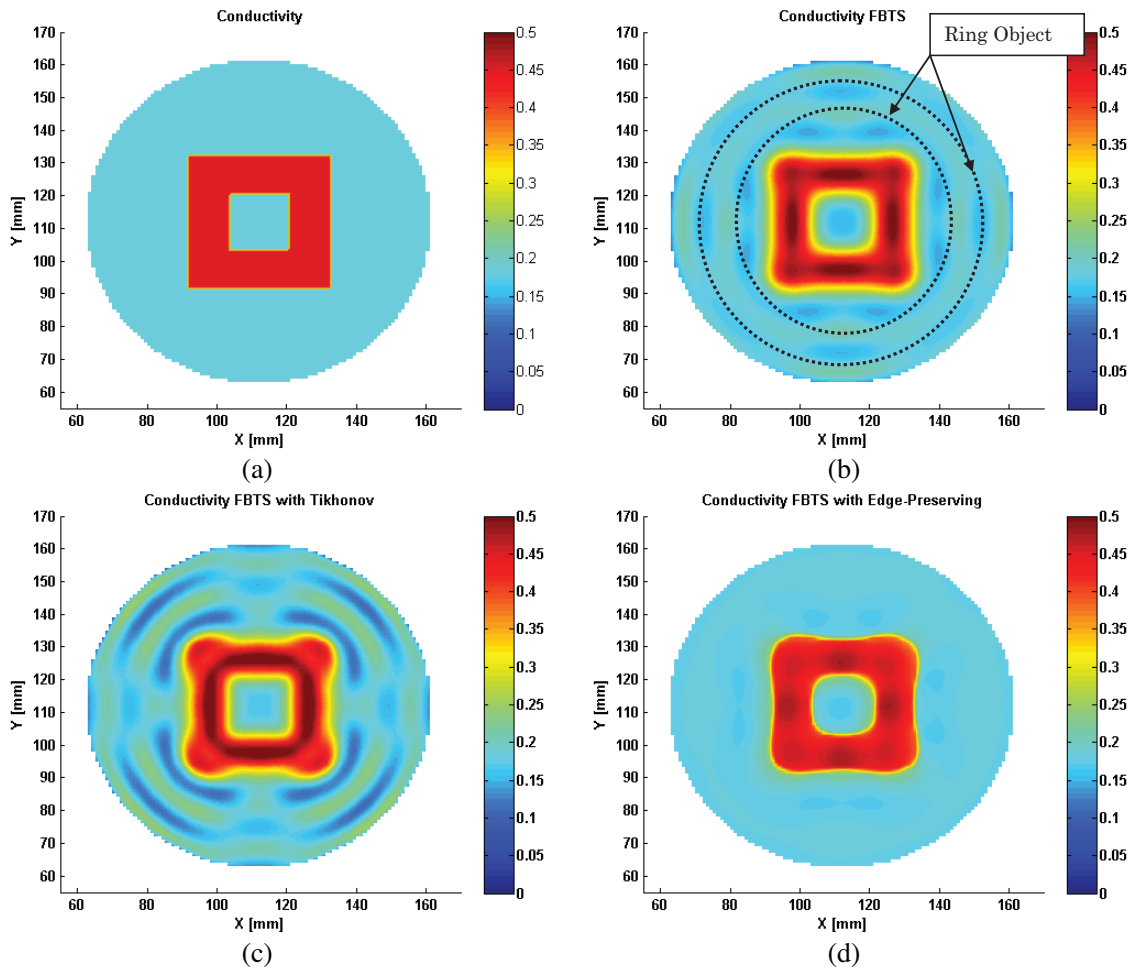


Figure 3. Conductivity profile: (a) Original profile. (b) Reconstructed profile by FBTS method. (c) Reconstructed profile by FBTS with Tikhonov regularization technique. (d) Reconstructed profile by FBTS with automated edge-preserving regularization technique.

the edges of the object can be observed as illustrated in Figure 2(b). As for the reconstruction of conductivity, the reconstructed image having a rough surface within the ROI. Two unknown ring objects are marked in dotted circle as illustrated in Figure 3(b). These reconstructed profile images give false reading where it may indicate that some other objects exist in the ROI. We believe that the results are trapped in local minima during the optimization process.

In order to avoid being trapped in local minima, regularization is needed. In this paper, the profile of reconstruction for two different regularization techniques is presented. The first one is the Tikhonov regularization technique, and the second is the proposed automated edge-preserving regularization technique. In FBTS with Tikhonov regularization technique, the reconstructed relative permittivity profile is improved as shown in Figure 2(c). However, for the reconstructed conductivity profile, the shape of the embedded object is changed from rectangle to circle, and the ring object in ROI can be clearly identified as shown in Figure 3(c). This occurs due to over-smoothing by the Tikhonov parameters.

In order to solve the over-smoothing effect, automated edge-preserving regularization technique is then proposed to preserve the edge while smoothing. As shown in Figure 2(d) and Figure 3(d), the FBTS with automated Edge-preserving regularization technique reconstructs more accurate profile than the other two techniques. In the result, no dotted area appears as shown in Figure 2(b), and there is no ring object presented in the ROI. It is believed that those false results are smoothed while maintaining the shape of embedded object. Thus, the FBTS with automated edge-preserving regularization technique provides a solution in smoothing the dotted area and ring object while preserving the edge of the embedded object.

In Figure 4, the cross-sectional views at axis $x = 107$ for relative permittivity and conductivity profiles are presented. It shows that the edges are smoothed when FBTS method is applied with the integration of Tikhonov regularization technique. However, the reconstructed results show that the ROI and embedded object are improved while the edges are preserved when FBTS integrated with automated edge-preserving regularization technique is applied.

The computed auxiliary variables for relative permittivity profile during simulation are obtained as illustrated in Figure 5. The initial step for the auxiliary variables is initialized as shown in Figure 5(a). The initial auxiliary variables at first iteration are assumed homogeneous and uniformly equal to 1. The weighting parameters λ are calculated automatically to the nearest decimal value of gradient as in Eq. (3). This will automatically stabilized both terms in Eq. (13).

At Step 1, new auxiliary variables are computed when the MSE for the current profile p^{n+1} and previous profile p^n is less than $1e-6$ as shown in Figure 5(b). The threshold values χ are calculated to determine the discontinuity or edge in the reconstructed profile. It is based on half of the highest value

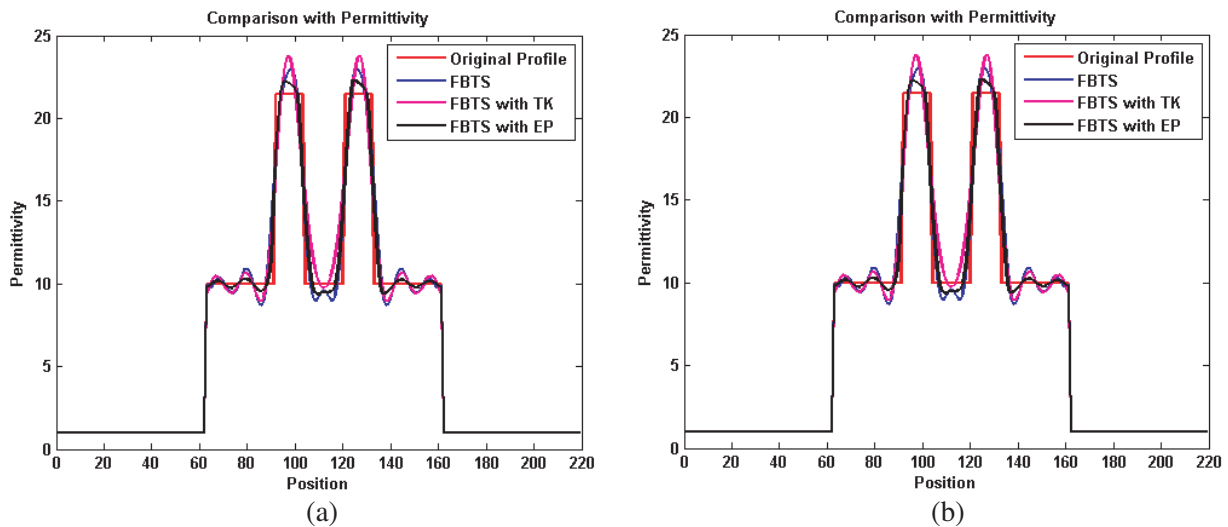


Figure 4. (a) Relative permittivity profile for cross-sectional view at axis $x = 107$. (b) Conductivity profile for cross-sectional view at axis $x = 107$.

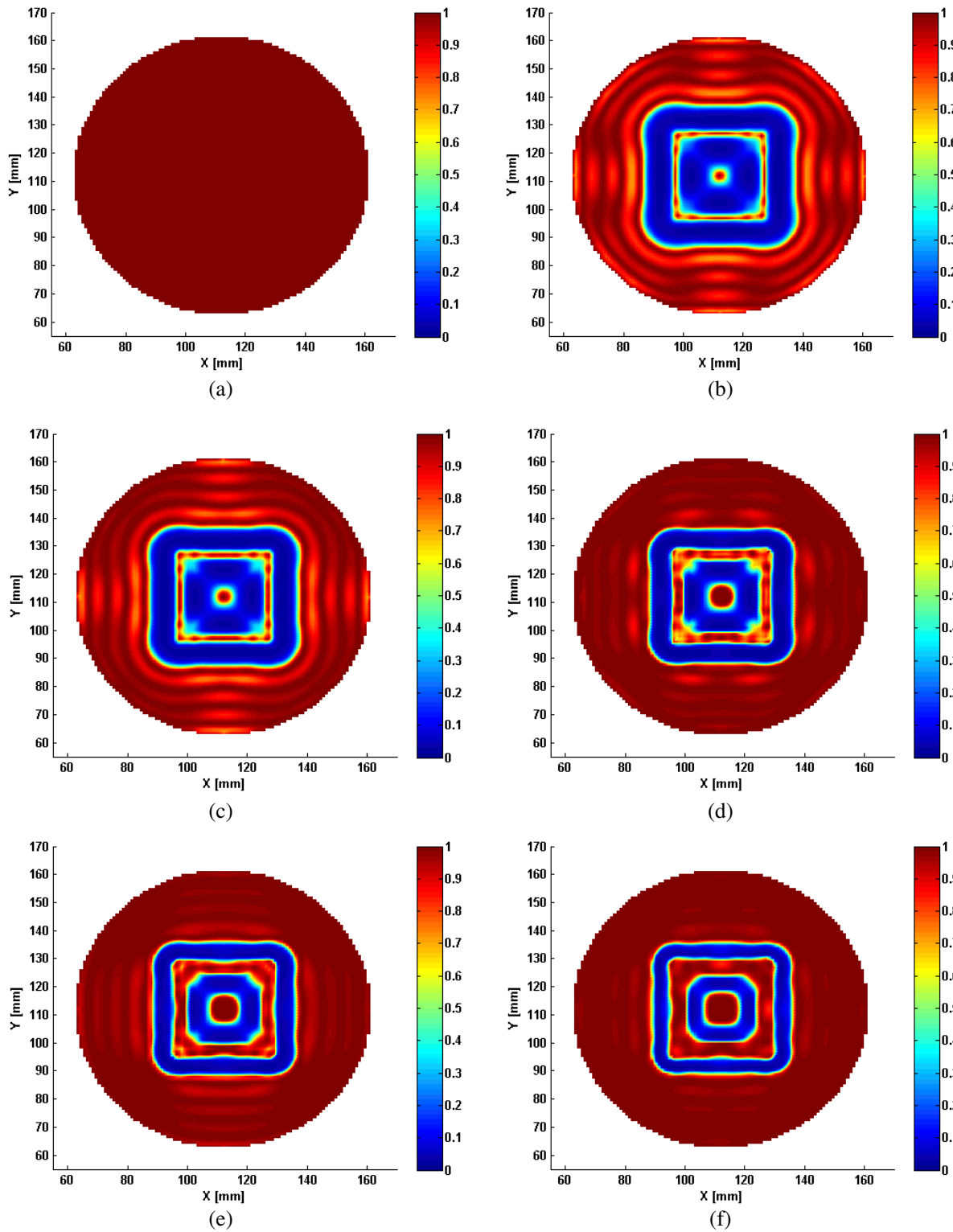


Figure 5. Auxiliary variables for relative permittivity. (a) Initial step, b^0 . (b) Step 1, b^1 . (c) Step 5, b^5 . (d) Step 15, b^{15} . (e) Step 30, b^{30} . (f) Step 51, b^{51} .

of the norm of gradient $\|\nabla p\|$. If the values are higher than χ , it is assumed as edge and needs to be preserved. This discontinuity or edge maps are roughly estimated and introduced for following profile estimate, and so on.

As the DrMSE algorithm proceeds, the auxiliary variables will become more precise as shown in Figure 5. At each step, new auxiliary variables are introduced, and the profile reconstruction becomes closer to actual profile. The DrMSE procedure takes 51 steps to reconstruct the relative permittivity profiles. Figure 5(b) through Figure 5(f) give the auxiliary variables for steps 1, 5, 15, 30 and 51 which take part in the 50th, 70th, 103th, 133th, and 188th iterations, respectively. Meanwhile, DrMSE procedure takes 45 steps to reconstruct the conductivity profile.

Figure 2 through Figure 4, FBTS integrated with automated Edge-preserving regularization technique yields better accurate result than FBTS method only and FTBS integrated with Tikhonov regularization technique. It is also proven by using MSE comparison of reconstructed dielectric profile and original profile as shown in Table 1. It shows that FBTS with edge-preserving regularization technique gives the smaller error than the other two techniques. All three numerical simulations only take about 40 seconds per iteration.

Table 1. MSE comparison and time per iteration.

MSE	Relative Permittivity Profile	Conductivity Profile	Time per iteration
FBTS method	3.1085e-04	1.1505e-05	37 second
FBTS with Tikhonov regularization technique	1.1797e-04	4.4966e-06	38 second
FBTS with edge-preserving regularization technique	6.7612e-05	1.4303e-06	38.5 second

4. CONCLUSIONS

Since the inverse scattering problem has nonlinear and ill-posed nature, edge-preserving regularization is integrated with FBTS method to avoid being trapped in the local minima during the minimization of cost functional. In this paper, we use DrMSE algorithm to control the alternate minimization scheme. Besides, the weighting parameters λ and threshold parameters χ are automatically decided by automated procedures iteratively. From the results, the FBTS with automated edge-preserving regularization technique has been successfully reconstructed with more accurate relative permittivity and conductivity profiles than using FBTS method only and FBTS with Tikhonov regularization technique. Therefore, we will extend this research to focus on more complicated and/or realistic model for our future research works.

ACKNOWLEDGMENT

This research was supported by *Research Acculturation Collaborative Effort (RACE)* grant scheme (RACE/c(3)/1332/2016(5)).

REFERENCES

1. Pastorino, M., *Microwave Imaging*, 1st edition, John Wiley, Hoboken, N.J., 2010.
2. Kim, Y. J., L. Jofre, F. De Flaviis, and M. Q. Feng, "Microwave reflection tomographic array for damage detection of civil structures," *IEEE Trans. Antennas Propag.*, Vol. 51, No. 11, 3022–3032, 2003.
3. Benedetti, M., M. Donelli, A. Martini, M. Pastorino, A. Rosani, and A. Massa, "An innovative microwave-imaging technique for nondestructive evaluation: Applications to civil structures

- monitoring and biological bodies inspection,” *IEEE Trans. Instrum. Meas.*, Vol. 55, 1878–1884, 2006.
4. Langenberg, K. J., K. Mayer, and R. Marklein, “Nondestructive testing of concrete with electromagnetic and elastic waves: Modeling and imaging,” *Cem. Concr. Compos.*, Vol. 28, No. 4, 370–383, 2006.
 5. Randazzo, A. and C. Estatico, “A regularisation scheme for electromagnetic inverse problems: Application to crack detection in civil structures,” *Nondestruct. Test. Eval.*, Vol. 27, No. 3, 189–197, 2012.
 6. Qaddoumi, N., R. Zoughi, and G. W. Carriveau, “Microwave detection and depth determination of disbonds in low-permittivity and low-loss thick sandwich composites,” *Res. Nondestruct. Eval.*, Vol. 8, No. 1, 51–63, 1996.
 7. Kharkovsky, S. and R. Zoughi, “Microwave and millimeter wave nondestructive testing and evaluation — Overview and recent advances,” *IEEE Instrum. Meas. Mag.*, Vol. 10, No. 2, 26–38, 2007.
 8. Zoughi, R. and S. Kharkovsky, “Microwave and millimetre wave sensors for crack detection,” *Fatigue Fract. Eng. Mater. Struct.*, Vol. 31, No. 8, 695–713, 2008.
 9. Deng, Y. and X. Liu, “Electromagnetic imaging methods for nondestructive evaluation applications,” *Sensors*, Vol. 11, No. 12, 11774–11808, 2011.
 10. Zoughi, R., *Microwave Non-destructive Testing and Evaluation*, Kluwer, The Netherlands, 2000.
 11. Pastorino, M., “Recent inversion procedures for microwave imaging in biomedical, subsurface detection and nondestructive evaluation applications,” *Measurement: Journal of the International Measurement Confederation*, Vol. 36, No. 3–4, 257–269, 2004.
 12. Pastorino, M. and A. Randazzo, “Buried object detection by an inexact newton method applied to nonlinear inverse scattering,” *Int. J. Microw. Sci. Technol.*, Vol. 2012, 2012.
 13. Estatico, C., A. Fedeli, M. Pastorino, and A. Randazzo, “Buried object detection by means of a L p Banach-space inversion procedure,” *Radio Sci.*, Vol. 50, No. 1, 41–51, Jan. 2015.
 14. Rufus, E. and Z. C. Alex, “Microwave imaging system for the detection of buried objects using UWB antenna — An experimental study,” *PIERS Proceedings*, 786–788, Kuala Lumpur, Malaysia, Mar. 27–30, 2012.
 15. Hagness, S. C., “Microwave imaging in medicine: Promises and future challenges,” *Proc. URSI Gen. Assem.*, 53706, 2008.
 16. Semenov, S., “Microwave tomography: Review of the progress towards clinical applications,” *Philos. Trans. A. Math. Phys. Eng. Sci.*, Vol. 367, 3021–3042, 2009.
 17. Meaney, P. M., K. D. Paulsen, and D. College, “Challenges on microwave imaging supported by clinical results,” *Proc. Int. Work. Biol. Eff. Electromagn. Fields*, 10–14, 2010.
 18. Hassan, M. and A. M. El-Shenawee, “Review of electromagnetic techniques for breast cancer detection,” *IEEE Rev. Biomed. Eng.*, Vol. 4, 103–118, 2011.
 19. Wei, N. S., K. A. H. Ping, L. S. Yee, W. A. B. W. Zainal Abidin, T. Moriyama, and T. Takenaka, “Reconstruction of extremely dense breast composition utilizing inverse scattering technique integrated with frequency-hopping approach,” *ARPJ. Eng. Appl. Sci.*, Vol. 10, No. 18, 8479–8484, 2015.
 20. Salvad, A., M. Pastorino, R. Monleone, A. Randazzo, T. Bartesaghi, G. Bozza, and S. Poretti, “Microwave imaging of foreign bodies inside wood trunks,” *IST 2008 — IEEE Workshop on Imaging Systems and Techniques Proceedings*, 88–93, 2008.
 21. Colton, D. and R. Kress, *Inverse Acoustic and Electromagnetic Scattering Theory*, Springer, New York, 2012.
 22. Massa, A., D. Franceschini, G. Franceschini, M. Pastorino, M. Raffetto, and M. Donelli, “Parallel GA-based approach for microwave imaging applications,” *IEEE Trans. Antennas Propag.*, Vol. 53, No. 10, 3118–3127, 2005.
 23. Donelli, M. and A. Massa, “A computational approach based on a particle swarm optimizer for microwave imaging of two-dimensional dielectric scatterers,” *IEEE Trans. Microw. Theory Tech.*,

- Vol. 53, No. 5, 1761–1776, 2005.
24. Rekanos, I. T., “Time-domain inverse scattering using Lagrange multipliers: An iterative FDTD-based optimization technique,” *Journal of Electromagnetic Waves and Applications*, Vol. 17, No. 2, 271–289, 2003.
 25. Winters, D. W., E. J. Bond, B. D. Van Veen, and S. C. Hagness, “Estimation of the frequency-dependent average dielectric properties of breast tissue using a time-domain inverse scattering technique,” *IEEE Trans. Antennas Propagat.*, Vol. 54, No. 11, 3517–3528, 2006.
 26. Takenaka, T., H. Jia, and T. Tanaka, “Microwave imaging of electrical property distributions by a forward-backward time-stepping method,” *Journal of Electromagnetic Waves and Applications*, Vol. 14, No. 12, 1609–1626, 2000.
 27. Takenaka, T., T. Tanaka, H. Harada, and S. He, “FDTD approach to time-domain inverse scattering problem for stratified lossy media,” *Microw. Opt. Technol. Lett.*, Vol. 16, No. 5, 292–296, 1997.
 28. Ping, K. A. H., T. Moriyama, T. Takenaka, and T. Tanaka, “Two-dimensional forward-backward time-stepping approach for tumor detection in dispersive breast tissues,” *2009 Mediterranean Microw. Symp. (MMS)*, 1–4, 2009.
 29. Blanc-Feraud, L., P. Charbonnier, G. Aubert, and M. Barlaud, “Nonlinear image processing: Modeling and fast algorithm for regularization with edge detection,” *Proc. IEEE-ICIP*, 474–477, 1995.
 30. Lobel, P., C. Picbota, L. Blanc Feraud, and M. Barlaud, “Conjugate gradient algorithm with edge-preserving regularization for image reconstruction from experimental data,” *IEEE Antennas Propag. Soc. Int. Symp. 1996, AP-S. Dig.*, Vol. 1, 644–647, 1996.
 31. Chew Chie, A. S., K. A. Hong Ping, Y. Guang, N. S. Wei, and N. Rajae, “Preliminary results of integrating Tikhonov’s regularization in Forward-Backward Time-Stepping technique for object detection,” *Appl. Mech. Mater.*, Vol. 833, 170–175, Apr. 2016.
 32. Kaltenbacher, B., A. Kirchner, and B. Vexler, “Adaptive discretizations for the choice of a Tikhonov regularization parameter in nonlinear inverse problems,” *Inverse Probl.*, Vol. 27, No. 12, 125008, Dec. 2011.
 33. Qin, Y. M. and I. R. Ciric, “Dielectric body reconstruction with current modelling and Tikhonov regularisation,” *Electron. Lett.*, Vol. 29, No. 16, 1427, 1993.
 34. Calvetti, D., S. Morigi, L. Reichel, and F. Sgallari, “Tikhonov regularization and the L-curve for large discrete ill-posed problems,” *J. Comput. Appl. Math.*, Vol. 123, 423–446, 2000.
 35. Charbonnier, P., L. Blanc-Féraud, G. Aubert, and M. Barlaud, “Deterministic edge-preserving regularization in computed imaging,” *IEEE Trans. Image Process.*, Vol. 6, No. 2, 298–311, 1997.
 36. Yong, G., K. A. H. Ping, A. S. C. Chie, S. W. Ng, and T. Masri, “Preliminary study of Forward-Backward Time-Stepping technique with edge-preserving regularization for object detection applications,” *2015 International Conference on BioSignal Analysis, Processing and Systems (ICBAPS)*, 77–81, 2015.
 37. Hadamard, J., “Lectures on Cauchy’s problem in linear partial differential equations,” *Physiology*, 334, 1923.
 38. Hebert, T. and R. Leahy, “A generalized EM algorithm for 3-D Bayesian reconstruction from Poisson data using Gibbs priors,” *IEEE Trans. Med. Imaging*, 194–202, 1989.
 39. Green, P. J., “Bayesian reconstructions from emission tomography data using a modified EM algorithm,” *IEEE Trans. Med. Imaging*, Vol. 9, No. 1, 84–93, Mar. 1990.
 40. Geman, S. and D. E. M. Clure, “Bayesian image analysis: An application to single photon emission tomography,” *Proc. Stat. Comput. Sect.*, 12–18, 1985.
 41. Aubert, G., M. Barlaud, L. Blanc-Feraud, and P. Charbonnier, “A deterministic algorithm for edge-preserving computed imaging using Legendre transform,” *Proceedings of the 12th IAPR International Conference on Pattern Recognition (Cat. No. 94CH3440-5)*, 188–191, 1994.
 42. Charbonnier, P., L. Blanc-Feraud, G. Aubert, and M. Barlaud, “Two deterministic half-quadratic regularization algorithms for computed imaging,” *Proceedings of 1st International Conference on Image Processing*, Vol. 2, 168–172, 1994.